RESERVOIR MODELLING OF LAHENDONG GEOTHERMAL FIELD, SULAWESI - INDONESIA

Zakaria Z. Sumantoro[1], Angus Yeh[2], John P. O'Sullivan[2] and Mike J. O'Sullivan[2]

[1]Star Energy Geothermal (Wayang Windu) Ltd, Indonesia
zakaria.zamrud@gmail.com

[2] Department of Engineering Science, The University of Auckland, Private Bag 92019, Auckland 1142, New Zealand
m.osullivan@auckland.ac.nz

Keywords: *Lahendong, Indonesia, TOUGH2, geothermal, reservoir, modelling, natural state*

ABSTRACT

Lahendong is a geothermal system in North Sulawesi, Indonesia, which has been generating electricity since 2001. Since this field is likely to be developed further, it is important to perform reservoir modelling of Lahendong to improve understanding of the characteristics of the field and to provide better estimates of its production capacity.

The model discussed here tries to improve on the previous numerical model that was developed by Yani (2006). The model is extended in area and depth, and the grid is refined. The surface of the model follows the topography and an air/water equation-of-state is used so that the shallow zone at Lahendong, including the vadose zone can be represented.

Model results from natural state simulations are compared to the actual temperature data from pre-production wells. Calibration to improve the model was performed by adjusting parameters in the model, such as permeability, flow rate and enthalpy of the deep inflow. After much iteration a good match to the temperature profiles was obtained, although there is still room for further improvements.

1. OVERVIEW

Lahendong geothermal area (see Figure 1) is one of the geothermal fields located in North Sulawesi, Indonesia. It is located about 30 km south of Manado, the capital city of North Sulawesi province, at an elevation of about 750 m above sea level (masl) (Utami *et al*., 2004). According to Prabowo *et al*. (2015), Lahendong is located in a large volcanic area including the Tondano and Pangolombian calderas, and also surrounded by several active volcanoes such as Mount Lokon, Mahawu, Pangolombian, Lengkoan, Kasuratan and Tampusu.

Development of Lahendong was first performed in the 1980s, which made it the first geothermal field to be developed in the eastern part of Indonesia. Before that time, the development of geothermal fields in Indonesia was restricted to only Sumatra and Java. Currently Lahendong is the only operating geothermal power plant in Sulawesi and supplies up to 60% of the electricity required in the north and central Sulawesi region (Permana *et al*., 2015).

Lahendong has the characteristics of a low permeability, liquid-dominated, reservoir. The temperature of the reservoir may be as high as 350°C. The proven productive area is about 4 km^2, which is concentrated around Lake Linau. Lahendong has 4x20 MWe power plants installed. The first 20 MWe Lahendong I Power Plant has been operating since 2001, while the identical 20 MWe Lahendong II and III Power Plants have been generating electricity since 2007 and 2008, respectively (Koestono *et al*., 2010). The last 20 MWe Lahendong IV Power Plant has been operating since 2012 (Prabowo *et al*., 2015). By 2013, 29 wells had been drilled with depths ranging from 1,200 to 2,500 m (Atmojo *et al*., 2015).

Figure 1: Location of the Lahendong Geothermal Field in Sulawesi, Indonesia
(from http://www.lonelyplanet.com/maps/asia/indonesia/map_of_indonesia.jpg)

The rate of production of fluid from the 10 production wells at the Lahendong field is 1,100 t/h, consisting of 600 t/h of steam and 500 t/h of brine. For injection purposes, there is an injection cluster (LHD-7) located at the east of the main field which consists of three injection wells. The north area produces two-phase fluid with a dryness of 30-50% while the south zone produces almost dry fluid, with a dryness above 80% (Prabowo *et al*., 2015).

2. GEOLOGY DATA

Generally, Lahendong field is a part of the depression of Pangolombian caldera, which is located at the western margin of the bigger Tondano depression. The Tondano depression extends in the N-S direction for about 20 km and opens to the west. The smaller Pangolombian caldera has well-defined structures in its eastern part but is relatively open to the west (Koestono *et al*., 2010).

Geological mapping of Lahendong and its neighbor, Tompaso, was performed by Ganda and Sunaryo in 1982, then interpretation of aerial photos was made by Robert in 1987 and interpretation of Land Sat and aerial photos by Siahaan in 2000 (Siahaan *et al*. 2005). Based on a current geological map, the Lahendong field is positioned in the small Pangolombian caldera which has collapsed in the centre, resulting in the formation of volcano named Tampusu-Linau. The prominent structures in Lahendong are dominated by NE-SW and NW-SE fault trends (see Figure 2), resulting from the collision between the Eurasian Plate in the north, the Tomini micro plate in the south and the North Sulawesi arm (Siahaan *et al*., 2005).

According to Widagda and Jagranatha (2005), there are six tectonic components in the Lahendong Geothermal Field:

(i). The Pangolombian structure, at the edge of Pangolombian Caldera.
(ii). A NE-SW fault, as the major volcano axis. This fault is correlated with the Tondano volcanic depression boundary limit.
(iii). An E-W fault, as pivot of a secondary magmatic intrusion. This fault is a lateral and trans-current fault.
(iv). Several NW-SE faults, of tensional type, formed by the Lahendong graben, giving normal faults and good permeability (Robert, 1987, from Koestono *et al*., 2010).
(v). Some N-S faults, produced by young tectonic activity, giving normal faults and good permeability (Robert, 1987, from Koestono *et al*., 2010).
(vi). A circular structure, interpreted as a deep plutonic intrusion.

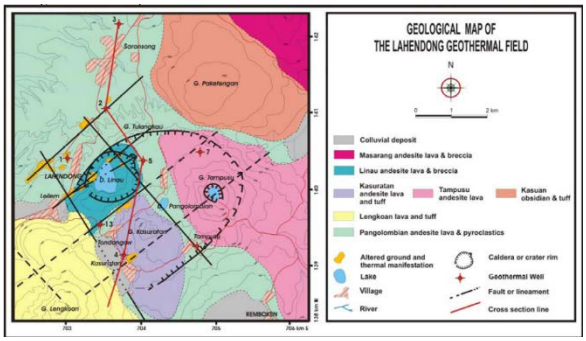

Figure 2: Geological map of Lahendong, with dominant NE-SW and NW-SE faults (Utami *et al*., 2004)

Based on the work of Widagda and Jagranatha (2005), the stratigraphy, from older to younger sequences, in Lahendong is as follows:

(i). Pre-Tondano, andesite, megaloclastics with sediment intercolation. From drilling, this formation was encountered at depths of 1,110-1,600 m.
(ii). Tondano, tuff and ignimbrite. From drilling, this formation was encountered at depths of 350-1,100 m.
(iii). Post-Tondano, consisting of 2 sub-units, the Pre-Pangolombian (basaltic and andesitic) and Post-Pangolombian (tuff and breccia). From drilling, this formation was encountered at depths of 0-850 m.

3. RESERVOIR CHARACTERISATION

The conceptual model of Lahendong geothermal field consists of two reservoirs, with the shallow reservoir at depths of 400-700 m and a deep reservoir below 1500 m (Widagda and Jagranatha, 2005). The shallow reservoir is found in wells LHD-1, LHD-2, pad LHD-4 and 5, indicated by lateral outflow from a shallow aquifer. The deep reservoir is characterised by the appearance of epidote, which usually corresponds to circulation losses during drilling, as found in wells LHD-5, LHD-7 and LHD-23 (Koestono *et al.*, 2010).

The Pangolombian and Pre-Tondano formations form the two productive reservoirs in Lahendong. The shallow reservoir is located in the vicinity of Lake Linau at 400 and 200 masl, and has a temperature of 250°C. The deep reservoir is located at about 1,100-2,300 m depth, and from the isobar map at 500 mbsl it can be seen that there is a strong geothermal fluid flow from south to north (Sumintadireja *et al*., 2001).

The reservoir rocks in Lahendong are mostly andesite, being part of the Pre-Tondano Unit. The reservoir is divided into two areas – the northern and southern – with the southern area have a higher reservoir temperature than the northern area (Koestono *et al*., 2010). The southern area has reservoir temperatures of up to 350°C, a pressure of 250 barg and a dryness of about 80%, while the northern area has reservoir temperatures of up to 250°C (see Figure 3), a pressure of 150 barg and a dryness of around 30% (Koestono *et al*., 2010). These two areas are separated by a N-S trending structure.

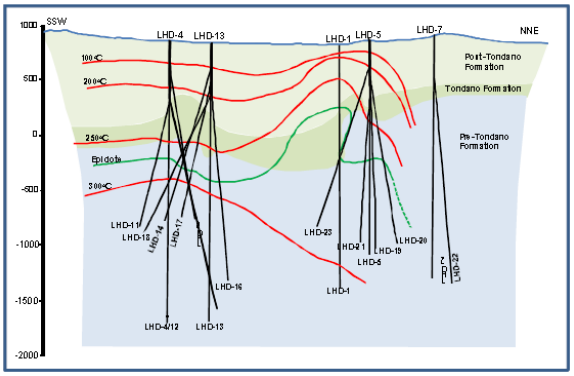

Figure 3: Formation and temperature distribution in Lahendong reservoir (Koestono *et al*., 2010)

The drilled wells are divided into two areas, with nine wells located in the northern sector and 12 wells in the southern zone, including three injection wells. There are also five wells that are located close to the boundary of the reservoir. Wells in the northern area are typically targeted at the Lake Linau Crater, while wells in the southern area are targeted at the southern zone fault system (Permana *et al*., 2015). Based on the data, the wells in the southern zone looked more promising than those in the north and so it was decided that the development would be focused in the south. Brine and condensate fluids are reinjected back into the reservoir through the LHD-7 cluster at a low temperature. Thus the LHD-7 cluster provides all the injection wells for the Lahendong system (Prabowo *et al*., 2015).

Table 1: Temperature profile interpretation for wells in the Lahendong system (after Yani, 2006)

Well	Indication from temperature profile
LHD-01	lateral hot water flow at the top (around 500 masl) and conductive flow temperature profile at the deeper elevation
LHD-02	conductive flow temperature profile
LHD-03	conductive flow temperature profile
LHD-05	heat conduction characteristics with lateral hot water flow at about 500 masl
LHD-06	heat conductive type, shows lateral flow of cold water at depths around 500 masl
LHD-07	the injection well has the lowest temperature in the field (max. temperature of 110 degC), and indicates down-flow of cold water
LHD-11	lateral cold water flow at around 0 m, while the temperature profile below 0 m shows a convective geothermal system
LHD-16	conductive flow temperature profile in the upper part
LHD-17	conductive flow temperature profile in the upper part
LHD-18	conductive flow temperature profile in the upper part
LHD-19	heat conduction characteristics with lateral hot water flow at about 500 masl
LHD-20	heat conduction characteristics with lateral hot water flow at about 500 masl
LHD-21	heat conduction characteristics with lateral hot water flow at about 500 masl
LHD-23	heat conduction characteristics with lateral hot water flow at about 500 masl

Most of the wells in Lahendong have temperature between 250 to 350°C, except wells LHD-3, 6 and 7 that all have temperatures below 150°C. These cool wells are located at the boundary of the geothermal system (Yani, 2006).

The well data for Lahendong geothermal system were gathered from the report by Yani (2006), which gave the pressure and temperature data for the wells taken before

production, or when they were still in natural state conditions.

According to the temperature profiles, summarised in Table 1, it can be deduced that the heat source of the reservoir is beneath the wells in pads LHD-4 and LHD-13 to the south of Lake Linau (see Figure 4). Furthermore, another heat source may be located close to well LHD-1 in the northern part of the field since it has a high temperature at 1000 mbsl (around 300°C), although it has low temperatures near the surface (Yani, 2006).

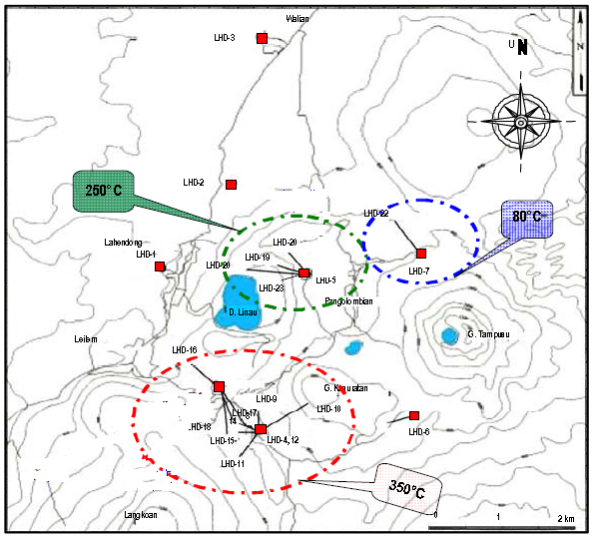

Figure 4: Locations of wells in the Lahendong geothermal field (after Yani, 2006)

4. NUMERICAL MODEL

The Lahendong geothermal system is owned and operated by Pertamina Geothermal Energy (PGE), and there are possibly several versions of a Lahendong reservoir model, that have been set up by PGE, internally (Yani, 2006). The present model makes use of geological, geophysical, geochemical (G3) and reservoir engineering data given in the technical data and reports produced by PGE. However, some updates and improvements are made to the previous models.

4.1 Model Design and Structure (Geometry File)

The design of the grid for the Lahendong model used in this study is based on the previous model by Yani (2006). That model covered an area of 121 km^2 (11 km in a NE-SW direction and 11 km in a NW-SE direction), which is larger than the known geothermal area. Its grid design consisted of 16 layers, where each layer is divided into 23 rows (NE-SW, x direction) and 20 columns (NW-SE, y direction). The total number of elements or blocks was 7,360. However, Yani's model did not consider the topography and instead used a constant elevation at the top surface, and covered an elevation from 800 masl to -2600 mbsl (Yani, 2006).

The present study tries to improve on the previous model by Yani (2006) in several respects:

(i). The size of the new model is extended to 12 km x 12 km covering an area of 144 km^2. The grid has 33 rows (NE-SW, x direction) and 33 columns (NW-SE, y direction), with a finer grid than the previous model (see Figures 5 & 6). The size of the grid blocks ranges from 500m x 500m down to 125m x 125m, with the finer grid located in the production and injection areas. The grid consists of 26 layers, with the thinnest layer being 50 m while the thickest is 300 m. The total number of elements or blocks is 20,740. Rectangular blocks are utilized in this model.

(ii). The orientation of the grid is NE-SW, rotated to the west by 28.9° from north, thus aligning the grid with the major fault in the area (NE-SW). Aligning the grid direction with the dominant fault helps in assigning the model parameters, such as in setting one horizontal permeability higher than the other.

(iii). The top of the model follows the topography (about 700-900 masl) and the base of the model is set at an elevation of 3000 mbsl (Figure 5). The thicknesses of the layers are not constant. The top layers are thinner because one of the objectives of this new modelling study is to represent the shallow unsaturated zone at Lahendong and thin layers are required to accurately represent the location of the water table. The deeper layers are thicker (see Figure 5).

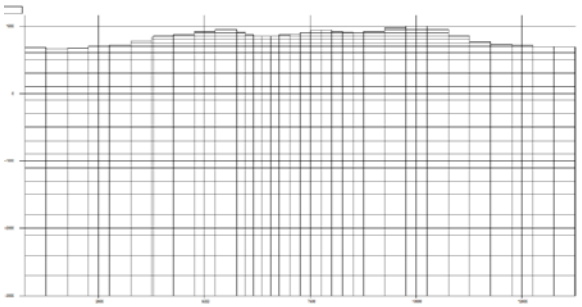

Figure 5: Vertical layers for the Lahendong model. The top of the model follows the topography and the base of the model is set at 3000 mbsl

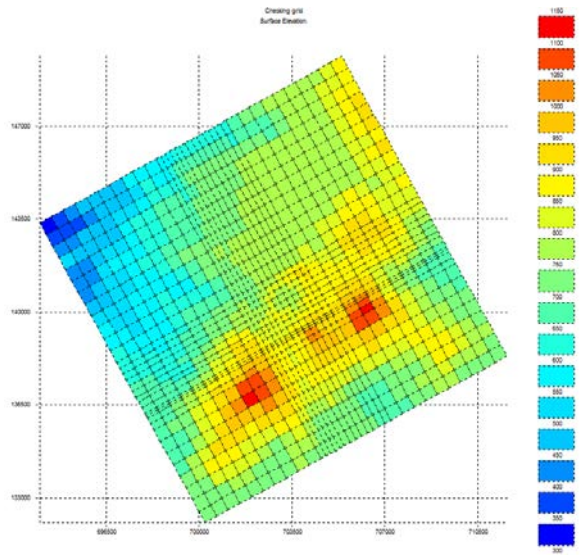

Figure 6: Plan view of the model, rotated to the west by 28.9^0 from north, and surface elevation of the Lahendong model (from high to low elevation: red to blue)

4.2 Rock Properties and Heat & Mass Flow

4.2.1 Rock properties

The data file contains rock properties and the deep heat and mass flows for the model. The rock properties are set up by deciding on the rock-types to be used in the model and their parameters such as density, porosity, permeability, thermal conductivity and specific heat. The assignment of the rock-types for each block in the model is also set in this data file.

The rock properties in the new Lahendong model were initially divided into three major rock-types: Pangolombian, Tondano and Pre-Tondano. Several identified faults were also included in the model and assigned their own rock-type. The rocks and faults for the model were assigned based on the 3G data (geology, geochemistry, geophysics) and the conceptual model. All rocks and faults were assumed to have a rock density of 2500 kg/m^3, a thermal conductivity of 2.5 W/m.K and a specific heat of 1000 J/kg.K. The porosity value is assumed to be 10%.

4.2.2 Boundary Conditions

Some of the heat and mass flows into or out of the model were also set. The deep heat and mass flows were set at the blocks at base (bottom layer), while cold inflows from rain infiltration were set at the blocks at the surface layer. The outflows from the surface manifestations were also set at some of the top layers.

Top Boundary

Atmospheric conditions are assigned at the top surface in block "ATM 0" (pressure of 1 bara and mean annual temperature of 25°C). An annual rainfall of 3,187 mm/year (based on actual rainfall data in Lahendong area) and an infiltration rate of 10% are used. Rainfall is represented by an inflow of cold water injected into the top of model with an enthalpy of 104.8 kJ/kg (25°C).

Side Boundary

All the side boundaries are assumed to be no-flow boundaries. This means there is no heat or mass coming into or out of the system. The side boundaries are located far from the potential active system, which is located around Lake Linau. In production history and future scenario simulations side recharge could be added.

Base Boundary

A conductive heat flux of 80 mW/m^2 is applied across the whole system. Since the Lahendong geothermal system is a liquid dominated reservoir, mass inflows are specified at parts of the base of the model (Layer 17), distributed across several locations around the potential production area (see Figure 7). The determination of the best locations for the hot upflows is part of the model calibration process.

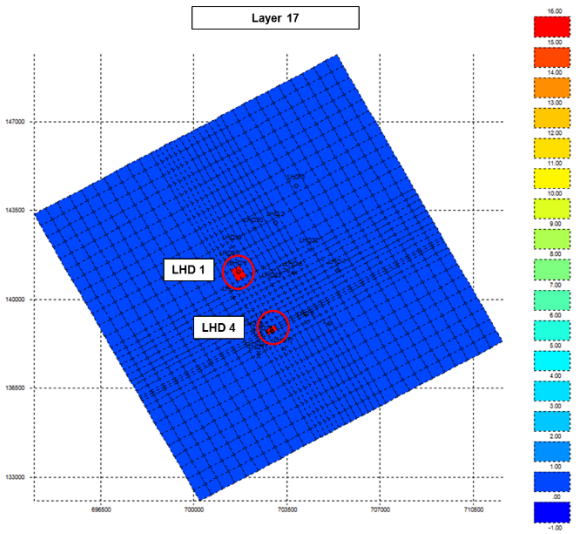

Figure 7: Initial mass flow location beneath LHD-1 and LHD-4 wells (red circles)

The enthalpy of the deep mass flow varies from 1500-1800 kJ/kg. Initially the mass flows were located at the points suggested by the conceptual model, mainly beneath LHD-1 and LHD-4. These sources provided a convective effect in the model and a maximum base temperature of about 320°C. However, during the calibration process, several adjustments were made and the mass flow was spread out into several locations. The total mass flow in this model is 90 kg/s.

Some hot springs were also represented in this model. There are 5 hot springs with a total mass flow of about 100 kg/s of water flowing out of the model.

4.2.3 Equations-of-State (EOS)

The equation of state used in this model is EOS3 (water, air). Air is approximated as an ideal gas, and for air and water vapour partial pressures in the gas phase are added:, Pg = Pa + Pv (Pruess *et al*., 1999). EOS3 is different from the other EOS modules in the choice of primary thermodynamic variables. In EOS3 with TOUGH2, the primary variables are (P, X, T) for single phase (liquid or gas), (Pg, Sg + 10, T) for two-phase (Pruess *et al*., 1999).

5. NATURAL STATE SIMULATION

The new Lahendong reservoir model was used to simulate the natural state conditions of the reservoir. The results from that simulation can be used to check whether the initial conceptual model is viable or not and to predict the reservoir conditions in the surrounding area as well as in the proven/drilled area. The unexplored area is of interest because it may have potential in the future.

To run the model the simulator AUTOUGH2 (Yeh *et al*., 2012) was used, which is a modified version of TOUGH2 (Pruess *et al*., 1998, 1999), a well-known heat and mass flow simulator. To show the simulation results, the graphical interface software MULgraph (O'Sullivan and Bullivant 1995) and TIM (Yeh *et al*., 2013) were used.

Each time the simulation was run and the output file of model results created, a comparison of temperature profiles from the simulation results and actual field data was made to determine the accuracy of the model. A PyTOUGH script (Croucher, 2011) was used to efficiently produce the comparison graphs as a single pdf file. Some examples of the initial results from the model are shown in Figure 8 below.

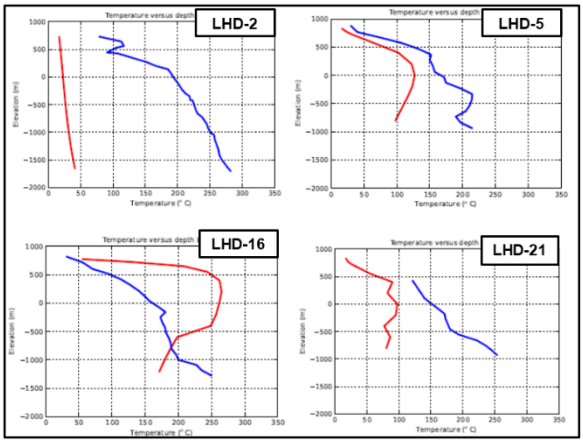

Figure 8: Initial temperature vs depth plots for wells LHD-2, 5, 16 and 21 (red: simulation results; blue: actual data)

From the figure above, it can be seen that the simulation results from this first model do not provide a good match to the actual data, and so further calibration was required to produce a closer match between the simulation results and the actual field data. The relatively poor results were expected because at the first stage of simulation the estimates of some parameters are based on limited and uncertain data. To improve the model, further calibration of the model was carried out.

6. MANUAL CALIBRATION PROCESS

In this study, the natural state calibration process involves matching temperature profiles from 16 exploration and exploitation wells in Lahendong.

Based on the results from the initial model, it can be seen that for most wells the model is too cold at the deep zone and is also inaccurate in the shallow zone. For the wells near the boundary e.g. LHD-2 and LHD-3, the temperatures are much too low, while for LHD-7 the temperature is much too high. A lot of improvements to the model needed to be performed in order to improve the match to the temperature profiles.

There are various strategies that can be applied in the manual calibration process, such as:

(i). Adjusting the deep inflows/mass flow locations at the bottom layer of the model (spreading out the mass flow). The initial location of the mass flow, based on conceptual model, was beneath LHD-1 and 4 but for calibration, distributing the mass flow may be a good idea as long as the total amount of mass flow injected into the model is maintained.
(ii). Adjusting the magnitude and enthalpy of the deep mass flow. This inputs more heat into the reservoir and increases the bottom temperatures.
(iii). Changing the permeability of the rock types. In the initial model, the assigned permeability is based on the best estimates from the conceptual model and 3G data. After comparing the results with field data, the permeability can be adjusted. As a starting point for model calibration, the rock-types were all assigned permeabilities of 0.1 to 50 mD. However, in the calibration process the permeabilities were changed, but within limits reasonable for a typical geothermal reservoir.
(iv). Adding new rock-types or new faults. The new rock/fault-types with new permeabilities could be introduced into the model in order to improve the match to the temperature profiles.
(v). Changing the other parameters of the rock-types, such as porosity, rock density, thermal conductivity and specific heat. However, time limitations for this study meant that this strategy could not be applied effectively.

In the early phase of the calibration process, the work was focused on spreading out the deep mass flow. Underneath some wells, especially a cluster with more than one well, deep mass flow was added and vertical permeability (z-axis) was also increased to allow the mass to flow more easily from the bottom to the top of the model. Some wells have a temperature about 300°C at a depth of 1000 mbsl, and so the hot fluid from the bottom layer (3000 mbsl) should flow directly to that depth.

The amount of the mass flow was also adjusted to control the heat input. Most of the upflow blocks have 1-3 kg/s of mass flow, but generally the total mass flow from the bottom was maintained, not exceeding the total from the conceptual model (90 kg/s). Furthermore, the enthalpy of some deep mass flow was adjusted to regulate the temperature near the bottom layer.

Some progress was made in improving the early model results, although the model was still not good enough. To improve the model, new rock types were introduced, especially beneath some wells, but still the match was not good enough.

As an experiment the lateral permeability was set higher. The permeability of the main rock types (CAPRO, PRETO, TONDA) was also modified at this phase. After these modifications a generally good match was obtained, but to improve some specific details further calibration should be performed.

For further calibration, for each well the temperature profile should be analysed carefully to determine how to obtain the best fit model for them. For instance, at LHD-1, 2 and 3, calibration was performed by modifying the permeability of each block beneath the wells to make sure that the temperature profile matches the actual data. For LHD-21 and 23, to get a better profile, changes were made in the permeability of the shallow blocks. Consequently, the temperature profiles for LHD-19 and 20, which have similar rock-types at shallow depth, became worse. For wells that are located close to each other, especially those which are located in the same cluster, a good match for all wells cannot be achieved, and so either a compromise should be accepted in this case or further refinement of the grid is required.

7. FINAL MODEL RESULT

After several steps of calibration and many AUTOUGH2 runs, a satisfactory match was obtained. Overall the model produces good results.

Since EOS3 (air-water model) is used in the model, a vadose zone is created at the elevation of around 700 masl. The vadose zone corresponds to the unsaturated zone above the water table where the vapour saturation > 0 and is located close to the surface (see Figure 9).

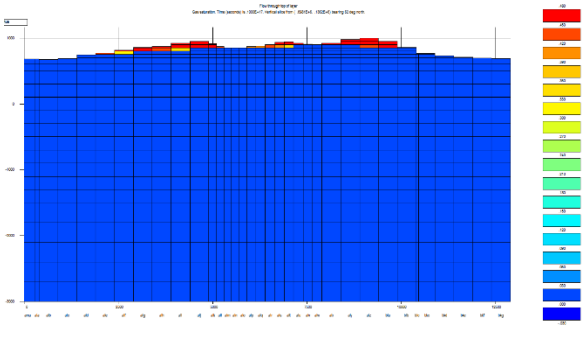

Figure 9: Vapour saturation plot showing the water table and vadose zone (from high to low vapour saturation: red to blue)

7.1 Final Rock Types and Properties

For the final rock-types and properties, several modifications were made to the initial rock-types and properties. Only the permeability was modified while the other properties are still

identical to the initial values. The permeability ranges from 0.001 mD to 100 mD. New rock-types were also added according to the requirements of the model, and their permeabilities were also varied.

Table 2: Final rock-types and permeability structure of the Lahendong Model

Rocks Type	Permeability (mD)		
	x	y	z
PANGO	10	10	1
PANGX	100	100	20
TONDA	0.01	0.01	0.01
TONDX	0.001	0.001	0.001
PRETO	0.1	0.1	0.05
PRETX	100	100	20
PRETY	0.01	0.01	0.01
PRETZ	100	100	100
CAPRO	0.1	0.1	0.1
FAUL1	50	7	5
FAUL2	10	5	2.5
FAUL3	10	5	5
FAUL4	50	5	5
FAUL5	1	1	1
FAUL6	50	50	30
FAUL7	0.1	0.1	5
FAUX7	0.1	0.1	1

Rocks Type	Permeability (mD)		
	x	y	z
FAUL8	70	70	50
FAUL9	70	70	50
FAU10	70	70	20
FAU11	2	50	5
FAU21	25	3.5	5
FAU22	5	2.5	30
FAU23	5	2.5	5
FAU24	25	2.5	5
FAU25	3.5	1	1
FAU26	25	25	30
FAU27	0.1	0.1	1
FAU28	1	1	1
FAU29	35	35	50
FAU30	35	35	50
FAU31	2	25	5
FAU32	5	2.5	2.5

7.2 Final Rock-type Assignments

For the final rock-type assignment, several modifications were made to the initial rock assignments. More faults from the conceptual model were introduced explicitly underneath some wells and above the deep heat flows, in order to get better temperature profiles. The data in Table 8 shows that a lot of new rock-types were assigned.

7.3 Final Temperature Distribution

From plots of the temperature distribution, it can be seen that the majority of the high temperature zone is caused by the deep heat flow beneath wells such as LHD-1, LHD-4 and LHD-5. The high temperature zone is concentrated in the centre of the model, which according to the conceptual model, is the potential geothermal production area.

It can be seen that, the isotherms for cross section C-C' (see Figure 10) from the simulation (Figure 11) looks similar to the isotherms from the conceptual model developed by Koestono *et al*. (2010), (Figure 12).

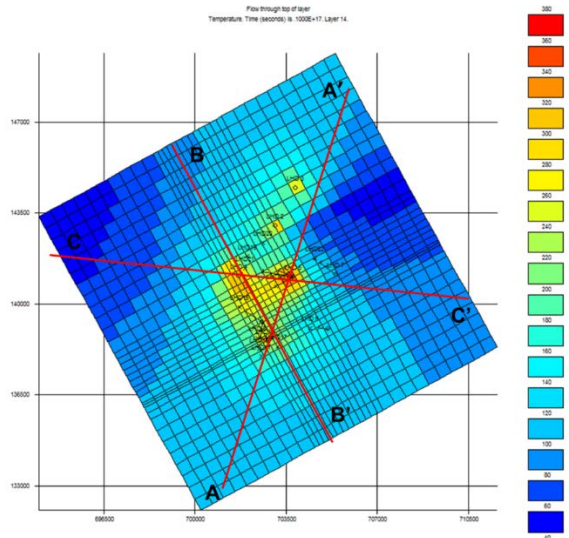

Figure 10: Spatial view of the temperature distribution in layer 14

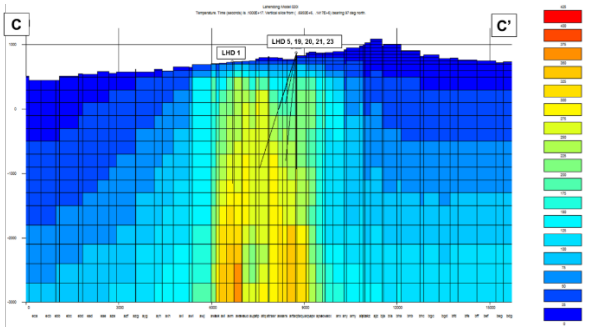

Figure 11: Vertical slice showing the temperature distribution on section C-C' (W-E)

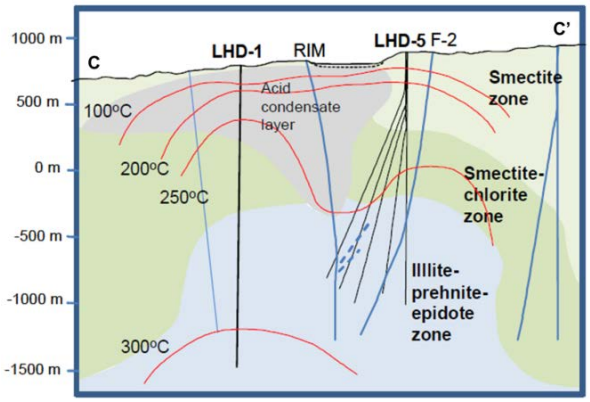

Figure 12: Vertical slice showing the isotherms from field data in Lahendong section C-C' (W-E) (after Koestono *et al*., 2010)

7.4 Final Mass Flow Location

For the final location of the deep mass flow, there were some changes from the initial settings. From only two local mass flows in the initial model, the mass flow in the final model is spread out over several locations in order to match the temperature profile of each well. The magnitude of each mass flow was varied, but the total mass flow injected to the model was maintained at the same level as the initial model, which was about 90 kg/s. The enthalpy of the deep upflow was adjusted slightly, but still kept in range between 1500 and 1800 kJ/kg.

7.5 Final Temperature Result

For the final temperature results, it can be seen that some improvements were achieved, compared to the initial results. There is still a challenge to match the profiles at shallow depths, since it is relatively hard to calibrate this zone.

7.6 Analysis of Natural State Simulation

From the final results it can be seen that some improvements have been made (see Figures 15, 16, 17 & 18). The maximum differences between the model results and well data are 50-70°C, although the close distances between several wells makes the calibration process challenging.

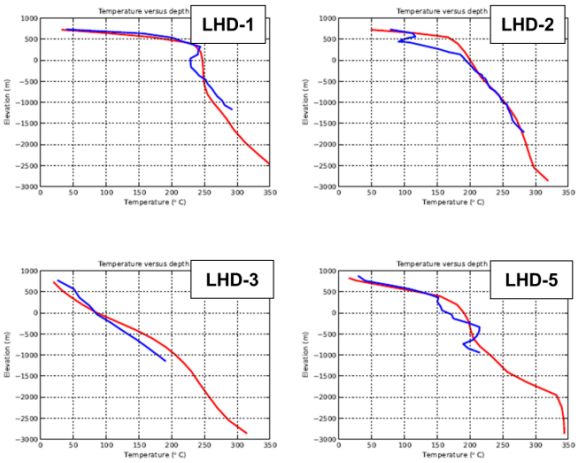

Figure 15: Final temperatures: LHD-1, 2, 3 and 5

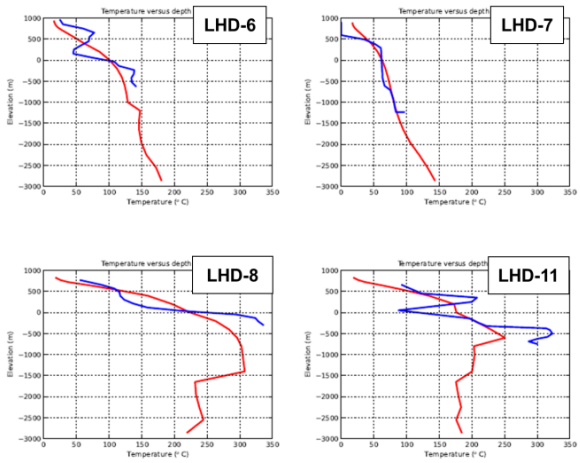

Figure 16: Final temperatures: LHD-6, 7, 8 and 11

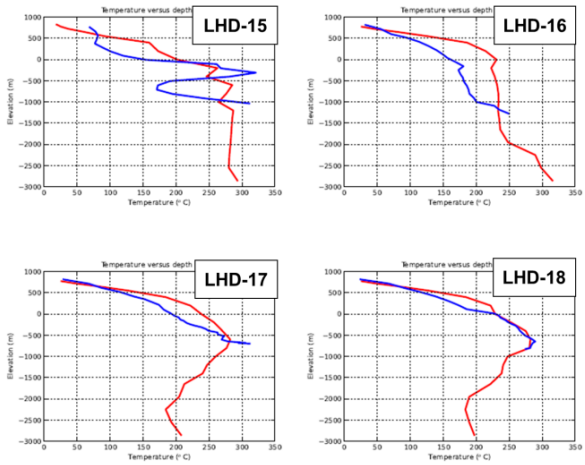

Figure 17: Final temperatures: LHD-15, 16, 17 and 18

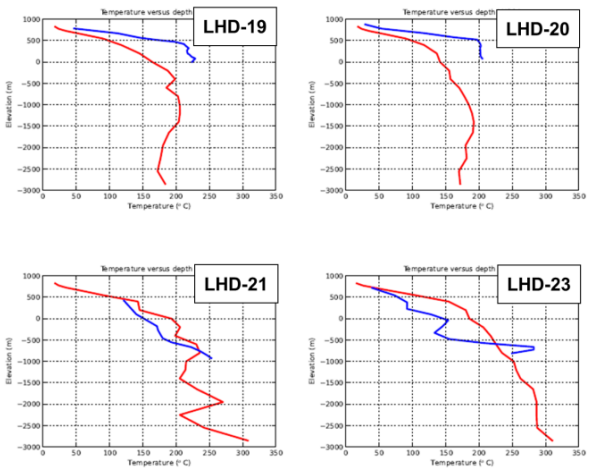

Figure 18: Final temperatures: LHD-19, 20, 21 and 23

It can be seen that the model temperature profiles for wells LHD-1, 2, 3 match the field data well. For LHD-1, in the conceptual model the deep mass flow was already assigned beneath that well, so there was not much calibration required in the model near this well. However, previously the temperatures for LHD-2 and 3 were too cold compared to the actual data (these wells are located at the border of resistivity boundary), but adding some deep mass flow beneath the wells and adjusting the permeability of the rocks along its depth made the profiles much better.

The example of a close distance between wells can be seen at the LHD-5 cluster, which consists of wells LHD-5, 19, 20, 21, and 23. While the shallow temperatures for LHD-19 and 20 show a good match, the profiles for LHD-21 and 23 are not so well matched. However, when calibration was used to improve the match for LHD-21 and 23, the match for LHD-19 and 20 became worse. The calibration was focused on the permeabilities of the shallow blocks around those wells. Since the shallow blocks for all the wells are same because they belong to a cluster, these results may be the best match that can be achieved without further refining the model.

There are some wells that have a large change in temperature over a small depth range, such as LHD-11 and 15. This makes calibrating the model harder, because the limitation of block size means there was not sufficient flexibility for adjusting the temperature profiles for these wells.

8. CONCLUSION

This study discussed an improvement of a natural state model of Lahendong geothermal reservoir system, which was based on a previous model by Yani (2006). Several adjustments were made to the Yani model such as expanding the total area and adding the actual topography to the model. The input data file parameters were also modified, including rock properties, permeability structure and deep mass flow.

The natural state model was calibrated manually by comparing the simulation result with the actual temperature data from pre-production wells. Various strategies were applied in calibration process, starting with general and moving to specific calibration. After many trials, a good match to the temperature profiles was obtained, although there is still room for further improvements. The results of the simulation indicate that the permeability of the reservoir varies in the range 0.1-100 mD, the enthalpy of the deep

inflow to the reservoir is about 1500-1800 kJ/kg and the total mass flow rate is around 80 kg/s.

Some challenges were met during the calibration process, such as the configuration of the wells in Lahendong where there is more than one well in a cluster, and the close distance between wells leads to difficulties in modelling all wells accurately. The large temperature difference over a small depth range in some of the actual temperature data also makes it difficult to match the temperatures with the existing vertical grid resolution.

9. RECOMMENDATION

Although an improved model of Lahendong was constructed in this study there is still further work that could be carried out to improve the model. For example:

(i). Set up a finer grid in order to accommodate more than one well in a cluster, allowing a better temperature profile to be obtained by adjusting the rock properties of each block.
(ii). Compare the results from manual calibration process with the results from an automatic calibration process using the iTOUGH2 software (Finsterle, 2007).
(iii). Collect more detailed data from well testing to get more accurate parameters for the reservoir simulation.
(iv). Collect the updated production data for the Lahendong wells, so the study can be extended to production history matching and future scenario simulations.

REFERENCES

Atmojo, J., Widarto, D., Kamah, Y., & Bramantyo, E.: Heat Source Movements in Lahendong Geothermal Field and Its Affect to the Reservoir Characteristics. *Proceedings World Geothermal Congress 2015*. Melbourne, Australia, 19-25 April, (2015).

Croucher, A.E.: PYTOUGH: A Python Scripting Library for Automating TOUGH2 Simulations. *Proceedings 33rd New Zealand Geothermal Workshop*. Auckland, New Zealand, 21 – 23 November, (2011).

Finsterle, S.: *iTOUGH2 User's Guide*. Report LBNL-40040, Lawrence Berkeley Laboratory, Berkeley, California. (2007).

Koestono, H., Siahaan, E., Silaban, M., & Franzson, H.: Geothermal Model of the Lahendong Geothermal Field, Indonesia. *Proceedings World Geothermal Congress 2010*. Bali, Indonesia, 25-29 April, (2010).

O'Sullivan, M., & Bullivant, D.: A graphical interface for the TOUGH family of flow simulators. *Proceedings of the TOUGH Workshop '95*, Berkeley, California. (1995).

Permana, T., Mulyanto, & Hartanto, D.: Geochemical Changes during 12 Year Exploitation of the Southern Reservoir Zone of Lahendong Geothermal Field, Indonesia. *Proceedings World Geothermal Congress 2015*, Melbourne, Australia, 19-25 April, (2015).

Prabowo, T., Yuniar, D., Suryanto, S., & Silaban, M. :Tracer Test Implementation and Analysis in Order to Evaluate Reinjection Effects in Lahendong Field. *Proceedings World Geothermal Congress 2015*, Melbourne, Australia, 19-25 April, (2015).

Pruess, K., Oldenburg, C., & Moridis, G.: Overview of TOUGH2, Version 2.0. *Proceedings TOUGH Workshop '98*. Berkeley, California, (1998).

Pruess, K., Oldenburg, C., & Moridis, G.: *TOUGH2 User's Guide, Version 2.0.* Lawrence Berkeley National Laboratory, Earth Sciences Division, Berkeley, California. (1999).

Sardiyanto, Nurseto, S., Prasetyo, I., Thamrin, M., & Kamah, M.: Permeability Control on Tompaso Geothermal Field and Its Relationship to Regional Tectonic Setting. *Proceedings World Geothermal Congress 2015*. Melbourne, Australia, 19-25 April, (2015).

Siahaan, E., Soemarinda, S., Fauzi, A., Silitonga, T., Azimudin, T., & Rahardjo, I.: Tectonism and Volcanism Study in the Minahasa Compartment of the North Arm of Sulawesi Related to Lahendong Geothermal Field, Indonesia. *Proceedings World Geothermal Congress 2005*. (2005).

Sigurdsson, H.: *Encyclopedia of volcanoes.* San Diego: Academic Press. (2000).

Sudarman S, Sumintadireja P. and Ushijima K.: Exploration of geothermal resources in Lahendong area, north Sulawesi, Indonesia, *Memoirs of the Faculty of Engineering Kyushu University*, 56, 3, 171-186. (1996).

Sumintadireja, P., Sudarman, S., & Zaini, I.: Lahendong Geothermal Field Boundary based on Geological and Geophysical Data. *Proceeding of The 5th Inaga Annual Scientific Conference & Exhibitions*. (2001).

Utami, P., Siahaan, E., Suroto, Azimudin, T., Browne, P., & Simmons, S.: Overview of the Lahendong Geothermal Field, North Sulawesi, Indonesia: A Progress Report. *Proceedings 26th NZ Geothermal Workshop*. Auckland, New Zealand, November, (2004).

Widagda, L., & Jagranatha, I.: Recharge Calculation of Lahendong Geothermal Field in North Sulawesi-Indonesia. *Proceedings World Geothermal Congress 2005*. Antalya, Turkey, 24-29 April, (2005).

Yani, A.: *Numerical Modelling Of Lahendong Geothermal System, Indonesia*. Project Report: United Nations University-Geothermal Training Programme, Iceland. (2006).

Yeh, A., Croucher, A., & O'Sullivan, M.: Recent Developments in the AUTOUGH2 Simulator. *Proceedings TOUGH Symposium 2012*. Berkeley, California, (2012).

Yeh, A., Croucher, A., & O'Sullivan, M.: TIM – Yet Another Graphical Tool For TOUGH2. *Proceedings 35th New Zealand Geothermal Workshop.* Rotorua, New Zealand, 17-20 November, (2013).